Title

Syndecan defines precise spindle orientation by modulating Wnt signaling in C. elegans

Journal

Development, 141(22)

ISSN

0950-1991

Authors

Dejima, Katsufumi
Kang, Sukryool
Mitani, Shohei
et al.

Publication Date

2014-11-15

DOI

10.1242/dev.113266

Peer reviewed

© 2014. Published by The Company of Biologists Ltd | Development (2014) 141, 4354-4365 doi:10.1242/dev.113266

RESEARCH ARTICLE

Syndecan defines precise spindle orientation by modulating Wnt signaling in *C. elegans*

Katsufumi Dejima[1,2], Sukryool Kang[3], Shohei Mitani[2], Pamela C. Cosman[3] and Andrew D. Chisholm[1,*]

ABSTRACT

Wnt signals orient mitotic spindles in development, but it remains unclear how Wnt signaling is spatially controlled to achieve precise spindle orientation. Here, we show that *C. elegans* syndecan (SDN-1) is required for precise orientation of a mitotic spindle in response to a Wnt cue. We find that SDN-1 is the predominant heparan sulfate (HS) proteoglycan in the early *C. elegans* embryo, and that loss of HS biosynthesis or of the SDN-1 core protein results in misorientation of the spindle of the ABar blastomere. The ABar and EMS spindles both reorient in response to Wnt signals, but only ABar spindle reorientation is dependent on a new cell contact and on HS and SDN-1. SDN-1 transiently accumulates on the ABar surface as it contacts C, and is required for local concentration of Dishevelled (MIG-5) in the ABar cortex adjacent to C. These findings establish a new role for syndecan in Wnt-dependent spindle orientation.

KEY WORDS: Heparan sulfate, Proteoglycan, Embryo, Endocytosis, Dishevelled, *C. elegans*

INTRODUCTION

Mitotic spindle orientation defines cell division orientation and plays crucial roles in animal development and tissue homeostasis (Gillies and Cabernard, 2011; Inaba and Yamashita, 2012; Lu and Johnston, 2013; Morin and Bellaiche, 2011; Siller and Doe, 2009). Aberrant cell division orientation is associated with neurological diseases and cancer (Noatynska et al., 2012; Pease and Tirnauer, 2011). Cells can orient their spindles according to default intrinsic rules, or in response to external cues. Wnt/Frizzled signaling is a widespread extrinsic cue for mitoticspindle orientation (Ségalen and Bellaiche, 2009). In the *C. elegans* early embryo, mitotic spindle orientation in the EMS and ABar blastomeres is regulated by directional Wnt/MOM-2 signals, acting in parallel to a Src-dependent pathway (Hardin and King, 2008; Park and Priess, 2003). EMS cell fate determination is also dependent on these pathways, in which a Wnt signal pathway regulates transcription in a β-catenin/WRM-1-dependent manner (Sawa and Korswagen, 2013). In contrast to cell fate determination of the EMS blastomere, spindle orientation of the EMS and ABar blastomeres is regulated in a β-catenin/WRM-1-dependent but transcription-independent manner (Cabello et al., 2010; Kim et al., 2013; Walston et al., 2004).

Although the above studies have shown the involvement of Wnt signaling in spindle regulation, it is not fully understood how Wnt signaling is spatially regulated to ensure precise spindle orientation. *In vitro*, a localized Wnt signal is sufficient to orient embryonic stem cell divisions (Habib et al., 2013). In *C. elegans* and vertebrates, Wnt signaling can be regulated at the subcellular level by controlling localization of downstream components (Lancaster et al., 2011; Mizumoto and Sawa, 2007; Taelman et al., 2010). However, how local transduction of a Wnt cue is established, maintained and terminated during mitosis is poorly understood.

Heparan sulfate proteoglycans (HSPGs) influence Wnt signaling and Wnt gradient formation in many systems (Lin, 2004). HSPGs are composed of negatively charged linear polysaccharides, composed of heparan sulfate (HS), which are attached to a core protein (Bishop et al., 2007). Interaction of HSPGs with Frizzled (Fz) receptors and Wnt ligands is thought to promote internalization of receptor-ligand complexes, which in turn either positively or negatively regulate extracellular Wnt ligand distribution and Wnt signaling (Gagliardi et al., 2008; Ohkawara et al., 2011). This biphasic activity of HSPGs is influenced by the ratio of ligand to receptor and co-receptors (Yan et al., 2009), the stability of free ligand (Kleinschmit et al., 2013) and possibly by specific HS structures (Ai et al., 2003). Additionally, the HSPG core protein can modulate signaling independently of or in conjunction with its HS side chains.

In *C. elegans*, HS synthesis is essential for embryonic morphogenesis (Kitagawa et al., 2007). However, the cellular role of HSPGs in embryonic morphogenesis has remained unclear. The membrane-spanning HSPG syndecan (SDN-1) has been identified as a negative regulator of Wnt/*egl-20* in distal tip cell migration (Schwabiuk et al., 2009), but it is not known whether HSPGs are involved in other Wnt-dependent processes. Here, we show that *C. elegans* embryos express the HSPG syndecan/SDN-1 from the one-cell stage onwards. We show that SDN-1 is required for a specific Wnt-dependent spindle orientation signal in the context of a newly formed cell-cell contact. Our results indicate that HSPGs can regulate precise spindle orientation by modulating Wnt signaling.

RESULTS

SDN-1 is the predominant HSPG core protein in the early embryo

To understand the roles of HSPGs in early *C. elegans* embryogenesis, we first examined the expression of total HSPGs by immunostaining. The antibody 3G10 (David et al., 1992; Minniti et al., 2004) recognizes stubs of HS chains formed by heparitinase cleavage, allowing the detection of all HS-modified proteins. We detected total HS (3G10) in one-cell stage embryos, which displayed patchy but specific 3G10 staining on the cell surface (Fig. 1Aa); at later stages, HS was concentrated at cell contacts (Fig. 1Ab-f,B; supplementary material Fig. S1A). We did not detect 3G10 staining in the absence of heparitinase treatment (Fig. 1B; data not shown). We noted that in two- and four-cell stage embryos, expression of total HS was higher in anterior cells (AB and ABa/

[1]Division of Biological Sciences, Section of Cell and Developmental Biology, University of California San Diego, 9500 Gilman Drive, La Jolla, CA 92093, USA. [2]Department of Physiology, Tokyo Women's Medical University, School of Medicine, 8-1, Kawada-cho, Shinjuku-ku, Tokyo 162-8666, Japan. [3]Department of Electrical and Computer Engineering, University of California San Diego, La Jolla, CA 92037-0407, USA.

*Author for correspondence (chisholm@ucsd.edu)

Received 23 May 2014; Accepted 3 September 2014

Development (2014) 141, 4354-4365 doi:10.1242/dev.113266

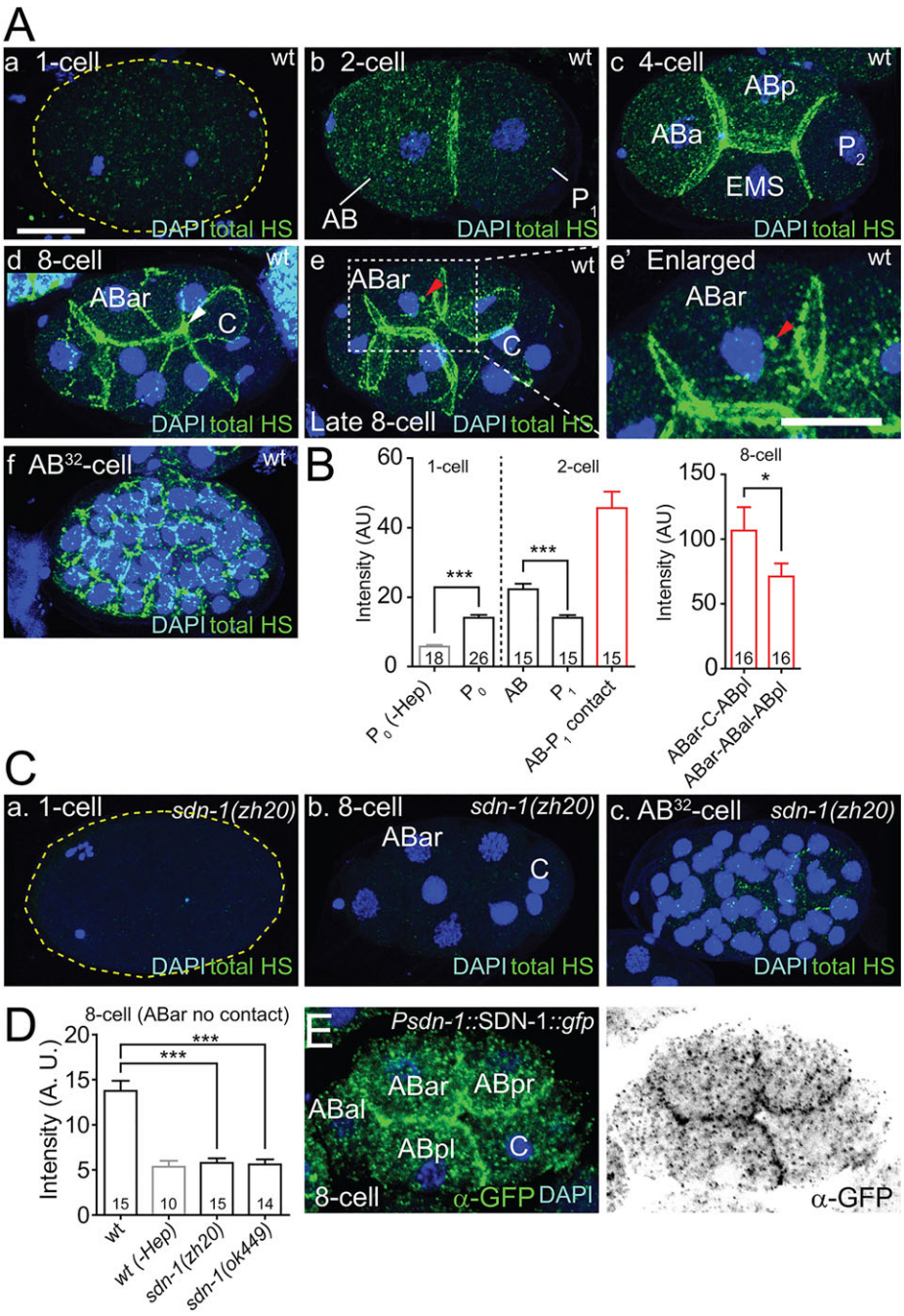

Fig. 1. Syndecan/SDN-1 is the predominant heparan sulfate proteoglycan in the early *C. elegans* embryo. (A) Expression of total HS in the wild-type early *C. elegans* embryo, as detected by staining with the anti-HS stub antibody 3G10; DAPI counterstain for nuclei. HS staining (green) is detectable at the one-cell stage (a; surrounded by a yellow dashed line); at the two-cell stage (b), HS is significantly enriched in AB compared with P_1. At the early eight-cell stage (d), HS accumulates on the contact site between ABar and C (white arrowhead); by the late eight-cell stage (e,e′), HS internalizes as a ~0.5 µm diameter particle in ABar (red arrowhead). At the AB^{32}-cell stage (f), HS is widespread in the embryo. (B) Quantification of cell surface 3G10 staining intensity in wild type, with (black or red bars) or without (gray bars) heparitinase treatment, and enrichment of HS immunostaining at the AB-P_1 cell contact and the ABar-C contact; data are arbitrary units (mean±s.e.m.). Red bars represent data obtained from cell-cell interfaces; black and gray bars represent data from regions away from cell contacts. Numbers in the bars represent the number of embryos. Student's-*t*-test was used to analyze data; **P*<0.05; ****P*<0.001. (C,D) Anti-HS (3G10) immunostaining is absent from *sdn-1(zh20)* embryos prior to the AB^{32}-cell stage. Confocal projections of 3G10 staining (C) and quantification (D) of cell surface staining on the contact-free cell surface of ABar in wild type and *sdn-1* mutants, and in embryos untreated with heparitinase (gray bar). One-way ANOVA and Tukey's test were used to analyze data. (E) Expression of SDN-1::GFP under the control of the *sdn-1* promoter and 3′UTR [*sdn-1(zh20); juSi119[Psdn-1-SDN-1::GFP-sdn-1 3′UTR]*] at the eight-cell stage; anti-GFP immunostaining is shown on the right. Scale bars: 10 µm. All images, except in E, are of embryos treated with heparitinase.

ABp) than in posterior cells (P_1 and P_2/EMS) (Fig. 1Ab,c). At the eight-cell stage (~30 min post first cleavage, pfc), we detected HS on the surfaces of all blastomeres. HS was distributed at most cell-cell interfaces, but was highly concentrated at the contact site between ABar and C (Figs 1Ad and 2). We noticed that during ABar mitosis, HS localized to an intracellular punctum in ABar, close to the ABar-C cell contact site (Fig. 1Ae). Expression of HS gradually increased during embryogenesis, and by comma stage (395 min pfc) was visible on the surface of almost all cells (supplementary material Fig. S1B).

C. elegans encodes multiple HSPG core proteins, of which syndecan/SDN-1 and glypican/GPN-1 are HS modified (Hudson et al., 2006; Minniti et al., 2004). To determine which core proteins are expressed in early embryos, we examined total HS expression in embryos lacking known HSPG core proteins using null or strong loss-of-function mutants. UNC-52/perlecan was not expressed in early embryos, as judged by MH3 antibody staining (not shown), confirming previous results (Mullen et al., 1999). 3G10 staining of *gpn-1(ok377)*, *lon-2(e678)* or agrin/*agr-1(tm2051)* embryos was indistinguishable from that of wild type (not shown). By contrast, 3G10 staining was undetectable in *sdn-1(zh20)* or *sdn-1(ok449)* embryos prior to the AB^{16} (28-cell) stage (Fig. 1C,D). In *sdn-1 (zh20)* embryos, we detected 3G10 staining in a few posterior cells at the AB^{32} stage, suggesting that expression of additional HSPGs begins between the AB^{16} and AB^{32} stages. We generated a functional SDN-1::GFP translational reporter under the control of its own promoter and 3′UTR (*juSi119*); using anti-GFP immunostaining, we detected SDN-1::GFP expression by the eight-cell stage (Fig. 1E), similar to the pattern of 3G10 staining. These observations suggest SDN-1 is the predominant HSPG core

Development (2014) 141, 4354-4365 doi:10.1242/dev.113266

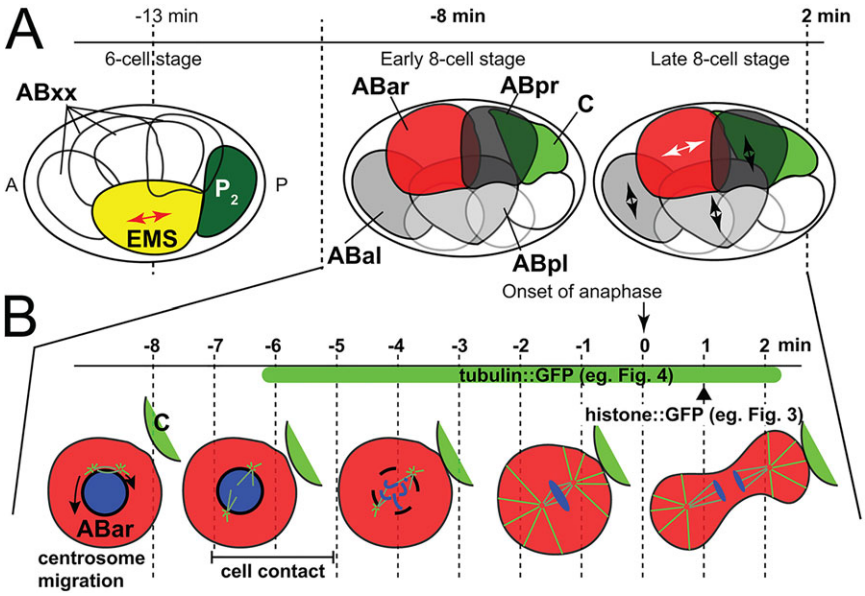

Fig. 2. Timecourse of ABar spindle reorientation and cell division in the wild type. (A) Diagrams of six- and eight-cell stage embryos showing orientation of EMS and ABxx division axes (bidirectional arrows); anterior is towards the right and dorsal is upwards. (B) Timing of ABar spindle reorientation relative to the onset of anaphase, defined as the beginning of chromosome separation (0 min). The ABar centrosomes start to migrate ~8 min before the onset of anaphase; by −7 to −6 min, the two centrosomes have reached opposite positions the nucleus. ABar begins to contact C at about −7 to −6 min. We analyze the ABar spindle by tracking centrosomal asters (TBB-2::GFP) from −5.5 min, or analyze the ABar division angle, as defined by the orientation of daughter nuclei (HIS-72::GFP) 1 min after the onset of ABar anaphase.

protein expressed in early embryos, and that SDN-1::GFP reflects endogenous SDN-1/HS expression.

HS synthesis and SDN-1 are required for proper ABar division orientation

SDN-1 is required for numerous aspects of post-embryonic development and morphology (Rhiner et al., 2005), and in ventral cleft closure during mid-embryogenesis (Hudson et al., 2006); however, it had not previously been implicated in early embryonic development. To assess the role of SDN-1 expression in the early embryo, we examined *sdn-1(zh20)* null mutant embryos using time-lapse DIC microscopy. *sdn-1* mutants developed normally until the eight-cell stage, and displayed normal orientation of the EMS division (Figs 2 and 3A,B; supplementary material Movies 1 and 2). However, the division axis of ABar was consistently misoriented in *sdn-1(zh20)*. We observed similar ABar division orientation defects in the HS synthesis mutants *rib-1(tm516)*, *rib-2(tm710)* and *hst-1(ok1068)* (Fig. 3C, supplementary material Movie 3; data not shown). In wild-type embryos, the ABar spindle undergoes a distinctive rotation so that ABar divides orthogonally to the axes of division of the other AB granddaughters: ABal, ABpl and ABpr. In HS synthesis and *sdn-1* mutants, ABar typically divided parallel to ABpr [five out of five embryos each for *rib-1(tm516)*, *hst-1(ok1068)* and *rib-2(tm710)*; eight out of 10 for *sdn-1(zh20)*]. These observations used visual estimation of the division axis or of the positions of daughter cells. To quantitate ABar division orientation more precisely, we used the NucleiTracker4D software (Giurumescu et al., 2012) to track histone-GFP labeled nuclei in 4D movies (Fig. 3D,E). This approach allowed us to plot 3D angles between the ABar and ABpr division axes, based on the positions of the GFP-labeled daughter nuclei immediately after chromosome segregation. This analysis revealed that, in wild-type embryos, the ABar-ABpr division axes were oriented at an angle of 91.5±12.9° (mean±s.d., n=21) 1 min after chromosome segregation (Fig. 3F; supplementary material Fig. S2A,B), consistent with our DIC microscopy observations and with previous studies (Walston et al., 2004). In the HS synthesis and *sdn-1* mutants, the angle between ABar and ABpr division was significantly decreased (Fig. 3F,G; supplementary material Fig. S2B), as was the ABar-ABal division angle (supplementary material Fig. S2C). By contrast, the angle between ABal and ABpl division axes was normal (Fig. 3F,G; supplementary material Fig. S2D). *sdn-1(RNAi)* embryos displayed a weaker ABar orientation defect (Fig. 3G). The division orientation defects of *sdn-1(zh20)* were fully rescued by SDN-1::GFP expressed under its endogenous control elements (91.0°±12.0, n=18, not shown). A mutant with a deletion in another HSPG core protein gene, *gpn-1*, showed normal ABar cell division orientation. *sdn-1 gpn-1* double mutants showed a slightly more severe ABar orientation defect than did *sdn-1* single mutants, although this was not statistically significant (Fig. 3G). As the ABar orientation defect of HS synthesis mutants is significantly more severe than that of *sdn-1*, additional HSPGs may contribute to ABar orientation. Taking our expression and mutant results together, we conclude that SDN-1 is the predominant HSPG required for normal orientation of the ABar cell division.

Previous embryological and genetic studies established that the mitotic spindle of ABar rotates in response to contact with and signaling from the C blastomere (Fig. 2) (Walston et al., 2004). The ABar-C contact is partly dependent on Wnt/MOM-2 (Pohl and Bao, 2010) and on the cell adhesion molecules L1CAM/SAX-7 and cadherin/HMR-1 (Grana et al., 2010). Using DIC microscopy, we observed that the ABar and C blastomeres form normal contacts in *sdn-1* mutant embryos, starting 5.6±0.4 min (mean±s.d., n=10) before the onset of anaphase in ABar, similar to the wild type (6.1±0.3 min, n=10). Likewise the ABar-C cell contact appeared normal in *rib-1* mutant embryos (supplementary material Movie 3). We conclude that neither SDN-1 nor HS are required for ABar to contact C, suggesting that the spindle orientation defects in these mutants arise from a failure in signaling.

SDN-1 is required for proper orientation of the mitotic spindle in ABar

To analyze ABar spindle orientation directly in these mutants, we labeled microtubules using GFP::TBB-2 (*ojIs1*) (Strome et al., 2001) and quantitated spindle dynamics, using NucleiTracker 4D software to track centrosomal asters. Previous studies indicated that the wild-type ABar spindle initially aligns parallel to the ABpr spindle, after which the aster closest to the ABar-C contact rotates to adopt the proper orientation before mitosis (Fig. 2) (Walston

Development (2014) 141, 4354-4365 doi:10.1242/dev.113266

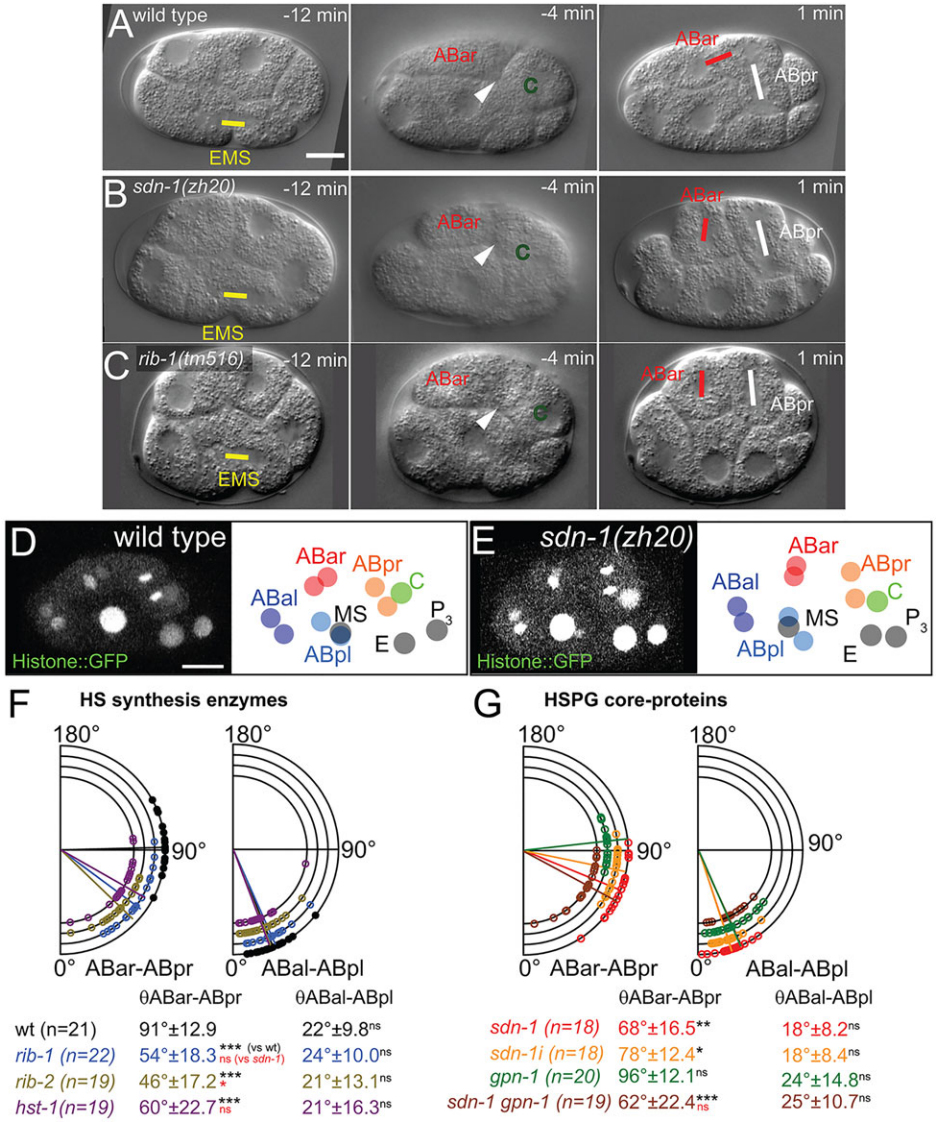

Fig. 3. HS synthesis and SDN-1 are required for proper orientation of the ABar division. (A-C) Orientation of the ABar division (red lines) is disrupted in *sdn-1* and *rib-1* mutants (B,C). DIC micrographs of wild-type (A), *sdn-1(zh20)* (B) and *rib-1(tm516)* (C) embryos at the six-cell stage (left; anaphase of EMS), the early eight-cell stage (middle; contact of ABar and C, white arrowheads) and the late eight-cell stage (right; anaphase of AB granddaughters). Orientations of the divisions of EMS (yellow lines) or ABpr (white lines) are normal in *sdn-1* and in *rib-1* mutants. Times are in minutes relative to the onset of ABar anaphase. Scale bar: 10 µm. (D,E) ABar daughter nuclei are mispositioned in *sdn-1* mutants, as detected by histone-GFP, and tracked by NucleiTracker4D. Representative images of HIS-72::GFP and 3D-projection models of wild-type (D) and *sdn-1(zh20)* (E) embryos. (F,G) The 3D angle between the ABar and ABpr daughters is ~90° in the wild type and is significantly reduced in HS synthesis (F) and in HS core protein mutants (G). The ABal-ABpl 3D angle is unaffected in these mutants. Mean angles and s.d. are listed under the graphs. *sdn-1i* indicates *sdn-1(RNAi)*. ANOVA and Tukey's tests were used to analyze data. ns, $P>0.05$, *$P<0.05$, **$P<0.01$ and ***$P<0.001$. The ABar division angle is defined by the orientation of daughter nuclei (HIS-72::GFP) 1 min after the onset of ABar anaphase.

et al., 2004). Under our imaging conditions, in which we use bead mounting to reduce embryo compression during imaging (Giurumescu et al., 2012), we found that in wild-type embryos ABar astral arrays were initially set up in variable orientations, and by metaphase become oriented towards the ABar-C contact independent of their initial orientation (Fig. 4A,B; supplementary material Movie 4).

To assess this observation quantitatively, we measured ABar spindle orientation relative to the AP axis of the embryo. In the wild type, the ABar spindle becomes oriented with the posterior aster dorsal and the anterior ventral. The ABar spindle axis also has a large left-right component, in that the posterior pole lies on the left-hand side of the embryo. In *sdn-1* mutants, the ABar spindle is initially variable in the AP, DV and LR planes, and rotates to an orientation that is consistent with respect to the AP-DV axis, but variable in the LR axis. Thus, ABar angles measured relative to the AP axis are initially variable but converge on an angle that is smaller than in the wild type (Fig. 4C-F). We also measured ABar orientation relative to the other AB granddaughters; ABar angles measured relative to the ABpr spindles were more variable in *sdn-1* mutants because of the larger LR component of these angles (data not shown). The mean orientation of the ABar spindle in *sdn-1* mutants was affected throughout the ABar cell cycle (Fig. 4E; supplementary material Movie 5). The abnormal spindle dynamics in *sdn-1(zh20)* were rescued by overexpression of SDN-1::GFP driven by the germline-specific *mex-5* promoter and the germline-permissive *tbb-2* 3′UTR (Merritt et al., 2008) (Fig. 4E). We also observed that overexpression of SDN-1::GFP resulted in significantly lower variance in the orientation of ABar astral arrays throughout mitosis without affecting mean orientation (Fig. 4F). These observations suggest SDN-1 is not required for spindle rotation per se, but modulates a cue that orients the astral microtubule array.

SDN-1 acts in a Wnt-dependent spindle orientation pathway

ABar spindle orientation requires two partly redundant signaling pathways: a Wnt pathway involving Wnt/MOM-2, Fz/MOM-5 and the Dishevelled proteins DSH-2 and MIG-5; and a receptor tyrosine kinase MES-1 that acts via Src/SRC-1 (Fig. 5A) (Walston et al., 2004). HSPGs, including syndecans, regulate Wnt signaling in many contexts (Lin, 2004; Munoz et al., 2006; Ohkawara et al., 2011), yet the involvement of HSPGs in Wnt-dependent spindle orientation has not been reported. Syndecan has also been implicated in Src-dependent stabilization of focal adhesions in fibroblasts (Morgan et al., 2013). To determine whether SDN-1

Development (2014) 141, 4354-4365 doi:10.1242/dev.113266

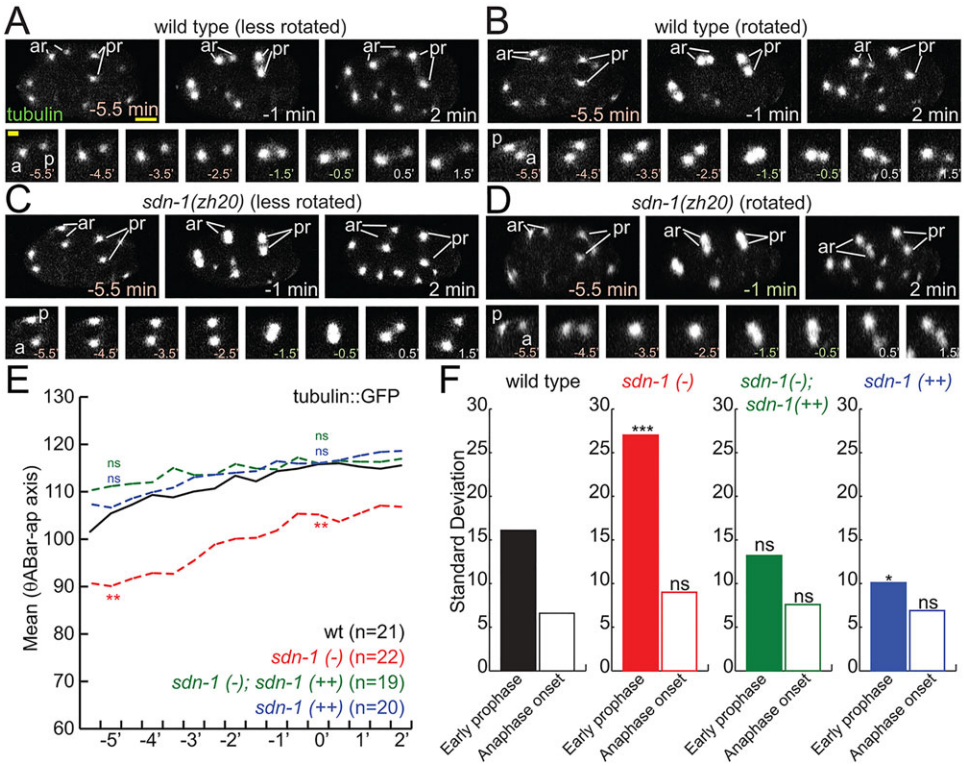

Fig. 4. SDN-1 constrains the orientation of the ABar spindle but is not essential for its rotation. (A-D) In the wild type and in *sdn-1* mutants, ABar spindles are initially set up with variable orientations. Two representative examples are shown from each genotype, in which centrosomes of ABar initially set up close to their final axis ('less rotated', A,C) or perpendicular to the final division axis ('rotated', B,D). 'ar' and 'pr' indicate the astral arrays of ABar and ABpr, respectively. Time-lapse images of GFP-labeled β-tubulin (TBB-2::GFP) in embryo (upper panels) or ABar (lower panels) of wild type (A,B) and *sdn-1(zh20)* (C,D). Time in minutes relative to onset of anaphase. Lower images show higher magnification views of TBB-2::GFP in ABar from the same embryos. 'a' and 'p' indicate the microtubule asters inherited by ABara and ABarp, respectively. Scale bars: 10 µm (upper panels) and 5 µm (lower panels). (E) To quantify the orientation of the ABar spindle in the anteroposterior/dorsoventral (AP/DV) plane, we calculated the angle θ between the axis of the ABar asters and the overall AP axis of the embryo. θABar mean is plotted over time relative to the onset of anaphase. The θABar mean in *sdn-1(–)* is significantly different at t=–5 min (early prophase) and 0 min (onset of anaphase), which is rescued by SDN-1::GFP. Data were analyzed using ANOVA followed by Dunnett's test: $^{**}P<0.01$. *sdn-1(–)* and *sdn-1(++)* indicate *sdn-1(zh20)* and an integrated single-copy transgene *juSi98[Pmex-5-SDN-1::GFP-tbb-2 3′UTR]*, which overexpresses SDN-1::GFP in the early embryo, respectively. (F) Bar graphs showing θABar standard deviation of indicated genotypes at t=–5 min (early prophase) and 0 min (onset of anaphase). The variance of ABar spindle orientation in the AP/DV plane is significantly higher in *sdn-1* than in wild type at the onset of anaphase, whereas it is smaller in *sdn-1(++)* (*F* test: $^{*}P<0.05$). The ABar spindle angle is calculated by tracking centrosomal asters (TBB-2::GFP) from –5.5 min prior to onset of ABar anaphase.

acts in the Wnt or Src spindle orientation pathways, we inhibited *dsh-2* and *mig-5* or *src-1* by RNAi in the wild-type and *sdn-1(zh20)* mutant backgrounds. When Wnt signaling was inhibited by *dsh-2 mig-5* double RNAi, the chromosome segregation angle between ABar and ABpr (Fig. 5B,C) but not between ABal and ABpl (not shown), was strongly reduced, consistent with previous reports (Walston et al., 2004). *src-1* RNAi had a similar, although weaker, effect (Fig. 5D). In *sdn-1(zh20) src-1(RNAi)* embryos, the angle between ABar and ABpr division was significantly reduced compared with *src-1(RNAi)* alone (Fig. 5D). By contrast, *sdn-1(zh20)* did not further enhance the ABar-ABpr division angle defect in *dsh-2 mig-5* double RNAi (Fig. 5C). The HS synthesis mutant *rib-1(tm516)* also displayed synergistic effects with *src-1(RNAi)*, but not with *dsh-2 mig-5* double RNAi (Fig. 5C). This pattern of synergism suggests HS-modified SDN-1 acts in parallel to the Src-dependent spindle orientation pathway, likely in the Wnt-dependent pathway. In addition, ABar spindle dynamics in *sdn-1(zh20) dsh-2 mig-5* double RNAi resembled those of *dsh-2 mig-5* double RNAi (Fig. 5E,F). These results suggest that the variable spindle rotation in wild type and *sdn-1* mutant depends on Dishevelled activity.

SDN-1 accumulates on the ABar protrusion and then at the ABar-C contact, and is then bi-directionally internalized into ABar or C

To address how SDN-1 modulates Wnt-dependent spindle orientation, we analyzed the dynamics of SDN-1 subcellular localization. The SDN-1::GFP transgene expressed under endogenous control elements (Fig. 1E) rescued the ABar division orientation defects of *sdn-1(zh20)* (supplementary material Fig. S5C,D), but its fluorescence level was too low for live imaging. For live imaging, we overexpressed SDN-1::GFP using the germline-specific *mex-5* promoter. P*mex-5*-SDN-1::GFP (*juSi99*) colocalized with the membrane marker pleckstrin homology domain PH::mCherry (Kachur et al., 2008) and appeared uniform on the surface of ABar and C at the six-cell stage (supplementary material Movie 6). To correlate SDN-1::GFP localization with cell division dynamics, we also expressed SDN-1::GFP with HIS-48::mCherry (supplementary material Fig. S3). When ABar was about to contact C, SDN-1::GFP began to accumulate on the tip of ABar closest to C (–1.6±0.3 min from cell contact, *n*=18, Fig. 6A); this SDN-1::GFP accumulation persisted 6.9±1.1 min after contact with C (*n*=18, Fig. 6B,D; supplementary material Fig. S5B). Three-dimensional reconstruction from orthographic views revealed

Development (2014) 141, 4354-4365 doi:10.1242/dev.113266

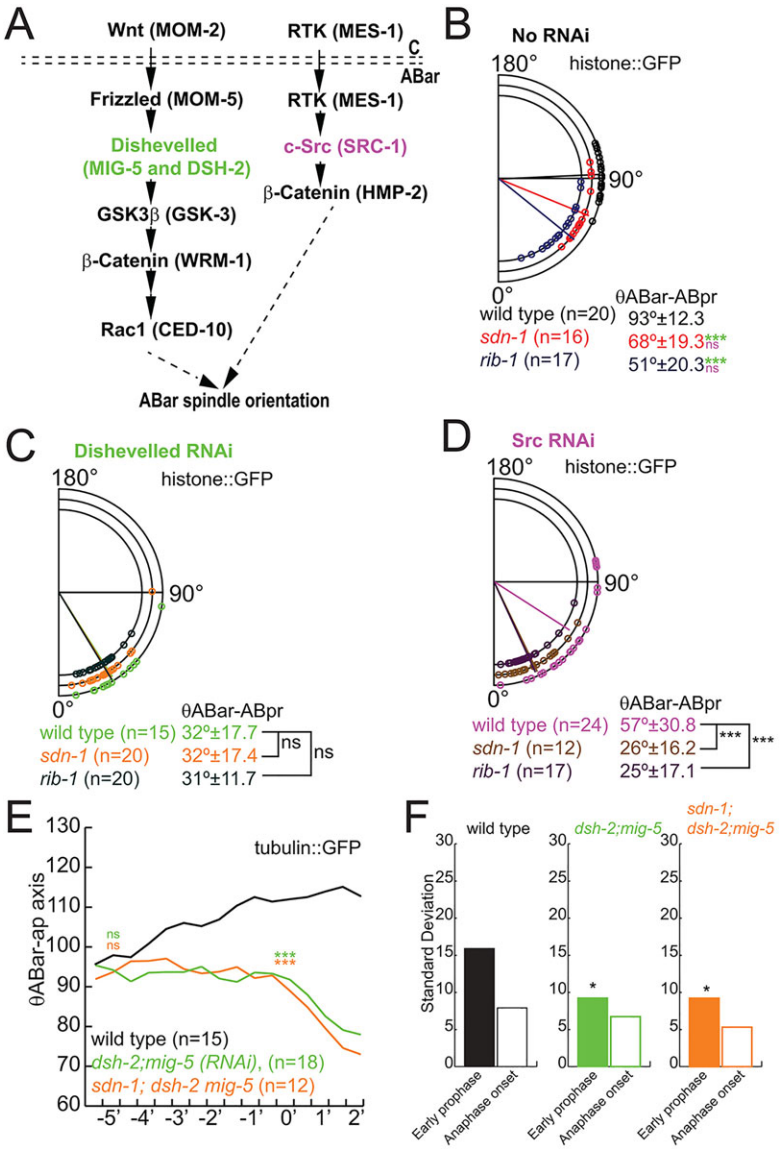

Fig. 5. SDN-1 functions in the Wnt-dependent ABar spindle orientation pathway and in parallel to SRC-1. (A) MOM-2/Wnt and SRC-1 pathways function in parallel to orient the ABar spindle (Cabello et al., 2010; Sumiyoshi et al., 2011; Walston et al., 2004). (B-D) Loss of function in *sdn-1* does not enhance ABar division orientation defects due to knockdown of Wnt signaling, and significantly enhances defects due to *src-1* knockdown. Circular scatter plots of the angle between ABar and ABpr division axes 1 min after onset of anaphase, obtained as in Fig. 3F,G. Mean angles and circular variance are shown below. ANOVA and Tukey post-hoc tests were used to analyze data: ns, not significant; ***P<0.001. Green asterisks in B are from a comparison between no RNAi and Dishevelled RNAi; the pink 'ns' comes from a comparison of no RNAi with *src-1* RNAi. (B) No RNAi, (C) Dishevelled *dsh-2 mig-5* double RNAi and (D) *src-1* RNAi in the indicated genotypes. (E) Time course of the angle θ between the axis of the ABar asters and the overall AP axis of the embryo. *dsh-2 mig-5* double RNAi both in wild-type and in *sdn-1(zh20)* embryos resulted in less ABar spindle rotation during prophase and metaphase. (F) Unlike loss of *sdn-1* (Fig. 4E,F), loss of Wnt signaling causes reduced variance (here shown as standard deviation) in initial ABar spindle orientation. Initial spindle orientation (t=−5 min) in *dsh-2 mig-5* double RNAi showed less variance compared with the wild type; F test, *P<0.05. The more variable orientation of ABar spindle prior to rotation in *sdn-1* mutant is not seen in *dsh-2 mig-5* double RNAi situation, suggesting that the effect is Wnt signal dependent. We analyze the ABar division angle, as defined by the orientation of daughter nuclei (HIS-72::GFP) 1 min after the onset of ABar anaphase (panels B-D), or the ABar spindle angle by tracking centrosomal asters (TBB-2::GFP) (E,F).

that SDN-1 accumulation on ABar has ABpr and/or ABpl immediately underneath it (Fig. 6A, right). Subsequently, SDN-1::GFP formed a ~0.5 µm diameter punctum either in ABar (13 out of 18, Fig. 6B) or in C (four out of 18, Fig. 6C, supplementary material Movie 7). These puncta may reflect internalization of the entire SDN-1 protein, as we observed similar structures using 3G10 immunostaining, which reflects endogenous SDN-1 HS chains (Fig. 1Ae). As the behavior of SDN-1::GFP-enriched puncta on ABar resembled that of midbody remnants (Singh and Pohl, 2014), we tested whether endogenous HS localizes to midbody remnants using the midbody marker ZEN-4::GFP. At the eight-cell stage, although the midbody remnant in P_2 (originating from P_1) did not contain HS, the midbody remnant localizing to the ABar-C interface showed strong HS expression (Fig. 6E), suggesting SDN-1 associates with a subset of midbody remnants.

How is SDN-1 enriched in the protrusion of the ABar blastomere? Syndecans are clustered by extracellular ligand stimulation through their HS side chains (Tkachenko and Simons, 2002). SDN-1 contains three potential glycosaminoglycan (GAG) attachment sites, i.e. Ser-Gly motifs; based on sequence context, only the first two Ser-Gly motifs are likely to be modified (Minniti et al., 2004). We expressed mutant forms of SDN-1, in which the first two putative GAG attachment sites were mutated (S71A, S86A or 2×S>A). When expressed under the control of the *mex-5* promoter, SDN-1::GFP induced strong expression of total HS in *sdn-1(zh20)* early embryos (supplementary material Fig. S4C). SDN-1(2×S>A)::GFP resulted in much weaker but detectable HS immunoreactivity in *sdn-1(zh20)* early embryos (supplementary material Fig. S4D), suggesting that although these GAG attachment sites are predominant, they may not account for all early embryonic HS. As the third potential GAG attachment site (S214) does not appear to contribute to early embryonic HS (supplementary material Fig. S4E), we conclude that S71 and S86 are the major HS modified sites in SDN-1, and that other sources of HS may account for the residual HS detected in these embryos (see Discussion). SDN-1 (2×S>A)::GFP enrichment on the ABar protrusion before cell contact was delayed relative to wild type (−0.7±0.2 min before cell contact, n=10, supplementary material Fig. S5B). The SDN-1 (2×S>A)::GFP accumulation remained 12.2±1.7 min after contact with C (n=10, supplementary material Fig. S5B).

We next addressed whether the intracellular domain of SDN-1 is required for SDN-1 dynamics. To test this, we examined GFP tagged-

Development (2014) 141, 4354-4365 doi:10.1242/dev.113266

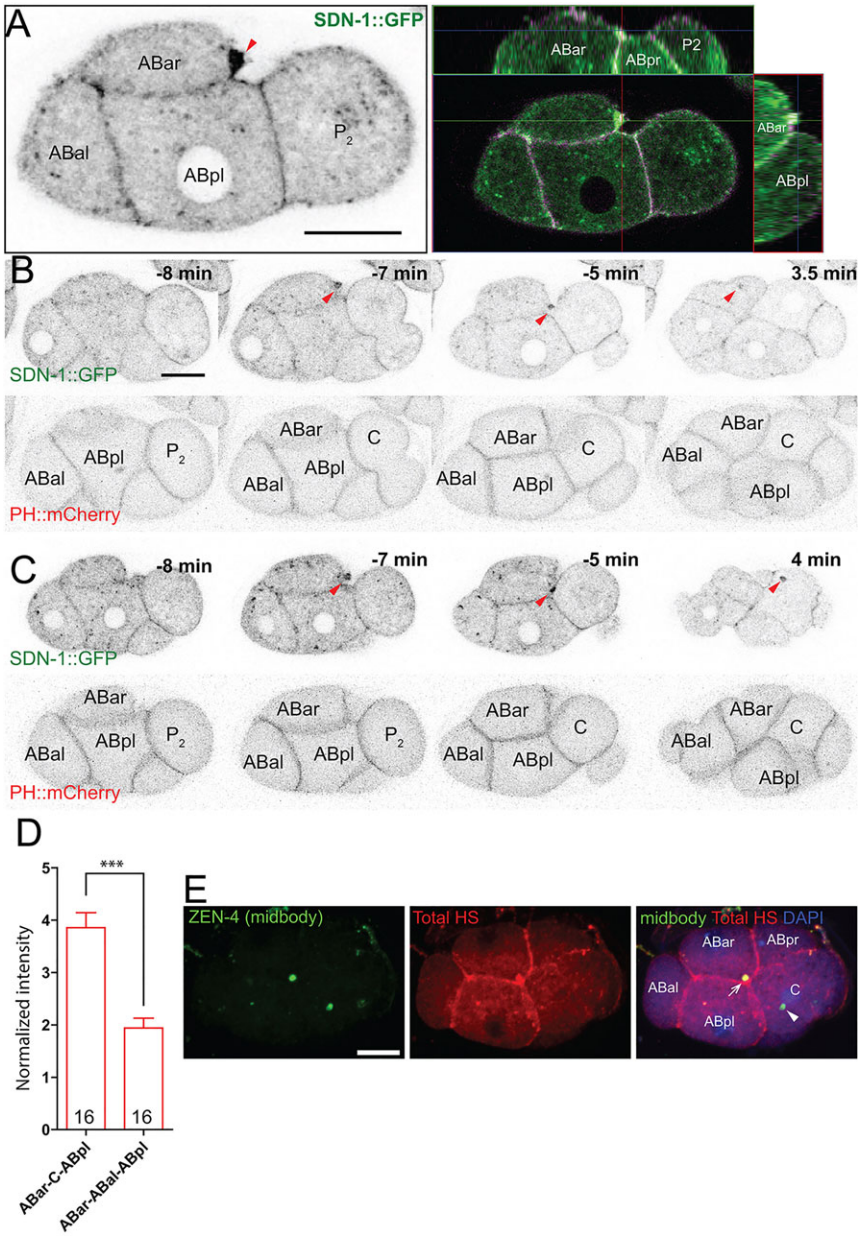

Fig. 6. SDN-1::GFP accumulates at the ABar-C contact site during ABar spindle orientation and is then internalized. (A) *Pmex-5*::SDN-1::GFP::*sdn-1 3′ UTR* (*juSi99*, left) in *sdn-1(zh20)* mutant background; images of single confocal slices of the eight-cell stage. SDN-1::GFP accumulation in the ABar blastomere is indicated by an arrowhead. An orthogonal view showing that SDN-1::GFP accumulation locates on contact between ABar and ABpr (right). (B,C) Time-lapse images of SDN-1::GFP (*juSi99*, focal plane, top) and PH::mCherry (*ltIs44*, 3D maximum intensity projection, bottom). Examples of SDN-1::GFP internalizing into ABar (B) or into C (C) are shown. (D) Accumulation of SDN-1::GFP at the ABar-C-ABpl contact is significantly higher than at the ABar-ABal-ABpl contact (Student's *t*-test, ***P<0.001). The intensity of SDN-1::GFP was normalized to PH::mCherry in each region of interest. (E) Accumulated total HS colocalizes with the midbody marker (ZEN-4::GFP, *ltIs43*), indicated by an arrow. Not all the midbody remnants contain HS accumulation (e.g. the midbody remnant from cell division of P_3 and C; arrowhead). To detect total HS, embryos were treated with heparitinase. We analyze the ABar spindle by tracking centrosomal asters (TBB-2::GFP) from −5.5 min, or analyze the ABar division angle, as defined by the orientation of daughter nuclei (HIS-72::GFP) 1 min after the onset of ABar anaphase.

SDN-1 lacking its cytoplasmic domain (SDN-1ΔC). Although SDN-1ΔC::GFP accumulated on the tip of ABar before cell contact (supplementary material Fig. S5B), endocytosis of this mutant form was delayed and less frequent compared with wild-type SDN-1::GFP (supplementary material Fig. S5B). We attempted to express SDN-1 lacking both its cytoplasmic domain and GAG attachment sites (S71A, S86A). However, this mutant form of SDN-1::GFP was not correctly localized on the cell surface (supplementary material Fig. S5A).

To address the importance of GAG modification and cytoplasmic domain of SDN-1, we next examined whether SDN-1ΔC::GFP and SDN-1(2×S>A)::GFP expressed under the control of the *sdn-1* promoter and 3′ UTR could rescue abnormal ABar spindle dynamics in *sdn-1(zh20)*. SDN-1::GFP (wild type) rescued both the variable initial spindle orientation and the continuously misoriented ABar spindle phenotypes of the *sdn-1(zh20)* mutant (supplementary material Fig. S5C,D). SDN-1ΔC::GFP rescued the variable initial spindle orientation, but failed to fully rescue the continuous misorientation of the ABar spindle, suggesting the SDN-1 cytoplasmic domain is required for precise spindle orientation regulated by Wnt. Correlating with its ability to restore low levels of HS expression, SDN-1(2×S>A)::GFP rescued both *sdn-1* phenotypes.

Wnt/MOM-2 defines the site of SDN-1 accumulation, which in turn is required for local accumulation of MIG-5/Dsh

To examine the effect of Wnt signaling on SDN-1 accumulation, we tested SDN-1::GFP dynamics in *mom-2* RNAi and *dsh-2 mig-5* double RNAi-treated embryos. Depletion of *mom-2* by RNAi eliminated SDN-1::GFP accumulation on ABar; instead, we observed premature SDN-1::GFP accumulation on C or ABpl during early prophase of ABar (Fig. 7B,C). We did not observe premature accumulation of SDN-1::GFP in *dsh-2 mig-5* double RNAi embryos (Fig. 7A,C), suggesting that MOM-2 engagement rather than downstream Wnt signal transduction defines the location of the site of SDN-1::GFP accumulation.

Development (2014) 141, 4354-4365 doi:10.1242/dev.113266

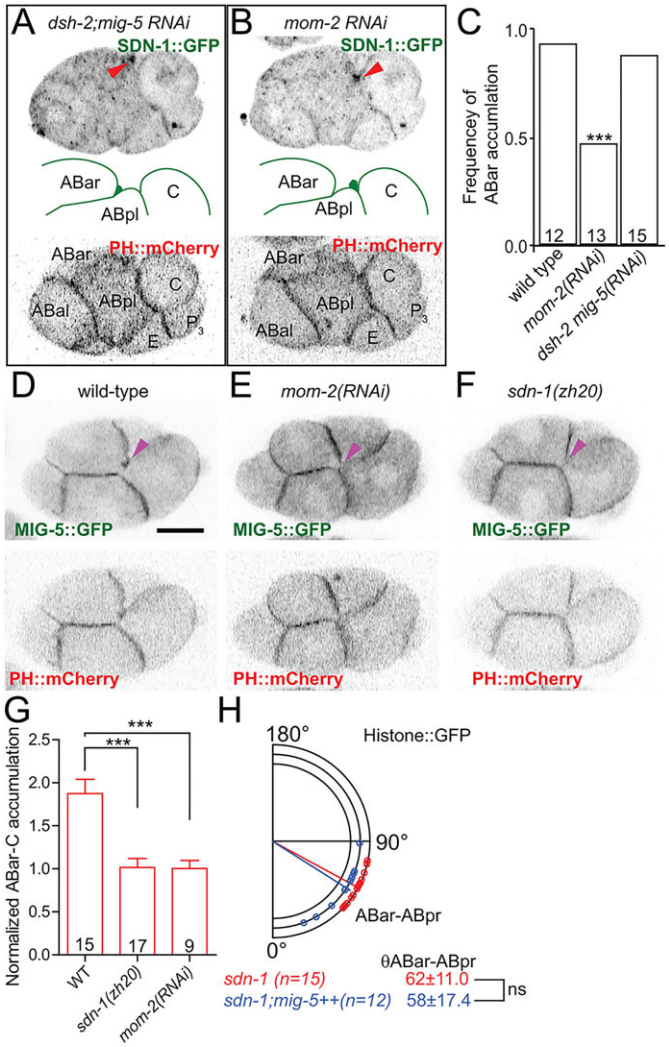

Fig. 7. Accumulation of SDN-1::GFP on the ABar-C contact site requires MOM-2/Wnt; SDN-1 is required for accumulation of MIG-5::GFP at the contact site. (A,B) In *dsh-2 mig-5* double RNAi embryos SDN-1::GFP accumulates on ABar (red arrowhead) as in the wild type (compare with Fig. 6A). *mom-2* RNAi resulted in failure in SDN-1::GFP accumulation on the ABar contact site; instead, premature SDN-1::GFP accumulated on the ABpl-C contact site before ABar contacts C, quantified in C. (D-F) 3D projections of embryos expressing MIG-5::GFP in wild-type (D), *mom-2* RNAi (E) and *sdn-1 (zh20)* (F) are shown. The ABar-C contact site is indicated by magenta arrowheads. In wild-type embryos, MIG-5::GFP accumulated after formation of the ABar-C contact (see also supplementary material Movie 8); *mom-2* RNAi and *sdn-1(zh20)* mutant embryos showed normal ABar-C contacts but did not accumulate MIG-5::GFP. (G) Quantification of MIG-5::GFP on the ABar-C contact site, normalized to PH::mCherry and expressed as a ratio of GFP intensity in the ABar-C-ABpl contact to the ABar-ABpl-ABal contact. Data are mean±s.e.m.; ***P<0.01. (H) Overexpression of MIG-5 (*juSi138[Pmex-5-MIG-5::GFP-tbb-2 3′ UTR]*) did not suppress the *sdn-1* division orientation defect. The ABar division angle is defined by the orientation of daughter nuclei (HIS-72::GFP) 1 min after the onset of ABar anaphase.

Finally, to examine the relevance of SDN-1 accumulation to downstream Wnt signaling, we followed the dynamics of a functional MIG-5::GFP (Wu and Herman, 2007). MIG-5::GFP expressed under the control of the *mex-5* promoter was enriched at the cortex in all cells of the early embryo, consistent with previous studies (Walston et al., 2006). In ABar, MIG-5::GFP accumulated similarly to SDN-1::GFP at the contact site with C (Fig. 7D; supplementary material Movie 8); however, unlike SDN-1::GFP, MIG-5::GFP accumulation was not observed before cell contact. MIG-5::GFP accumulation on the ABar-C contact site was reduced in embryos treated with *mom-2* RNAi, even in embryos where ABar-C contact occurred normally, suggesting that local accumulation of MIG-5::GFP might reflect activation of Wnt signaling rather than contact itself (Fig. 7E,G). Importantly, MIG-5::GFP accumulation on the ABar-C contact site was significantly reduced in *sdn-1(zh20)* (Fig. 7F,G), indicating that SDN-1 is required for MIG-5 accumulation. Dishevelled overexpression has been shown to rescue defective convergent extension caused by loss of *glypican 4* and *syndecan 4* in *Xenopus* (Munoz et al., 2006; Ohkawara et al., 2003). However, overexpression of MIG-5::GFP (4- to 5-fold overexpression; data not shown) did not rescue the ABar misorientation phenotype in *sdn-1(zh20)* (Fig. 7H), suggesting that SDN-1 localization does not simply enhance Wnt signaling but provides a positional cue.

DISCUSSION

This study reveals a highly specific requirement for syndecan in Wnt-dependent mitotic spindle regulation. Our results support a model in which SDN-1 functions in the Wnt signaling pathway, either at the level of Wnt/MOM-2 or Fz/MOM-5, to promote ABar spindle reorientation. Localization of SDN-1 on ABar requires MOM-2, and SDN-1 is required for localization of Dsh/MIG-5. Moreover, the difference between the *sdn-1* phenotype and the *dsh-2 mig-5* phenotype can be explained if SDN-1 restricts Wnt signaling. Speculatively, syndecan/SDN-1 on the ABar surface might concentrate either Wnt/MOM-2 or its receptor Fz/MOM-5. The HS side chains of SDN-1 might allow this process to begin prior to physical contact with the C blastomere, triggering SDN-1 clustering (Fig. 8). SDN-1 accumulation could concentrate Wnt/MOM-2 onto the ABar protrusion, which in turn weakly orients the mitotic spindle in ABar towards C. In addition, we have analyzed ABar spindle dynamics in *sdn-1(zh20) dsh-2 mig-5* double RNAi, and find that they resemble *dsh-2 mig-5* double RNAi, i.e. no spindle rotation. This epistasis test shows that the variable rotation in *sdn-1* mutants requires Dishevelled activity, consistent with our model. At present, reagents to visualize Wnts or their receptors in the early embryo are not available. Our attempts to generate MOM-2 transgenic animals have so far been unsuccessful, and antibodies to MOM-2 have not been generated. MOM-5::GFP expression is not detectable in the early embryo (Park et al., 2004). Wnt ligands and receptors may be expressed transiently or at low levels in the early embryo, necessitating the involvement of accessory proteins such as SDN-1. We do not yet know whether SDN-1 function is required in the Wnt-sending or Wnt-receiving cell, or both, and we cannot yet exclude models in which HSPG/SDN-1 enhances the Wnt signal by helping Wnt spreading, by serving as a trans co-receptor on other cells (e.g. ABpr/pl) or by causing Wnt secretion in the signal-sending cell (Sarrazin et al., 2011; Zhu and Scott, 2004).

The pathways required for spindle reorientation in EMS and in ABar have until now appeared to be almost identical (Thorpe et al., 1997; Walston et al., 2004). However, we find (at most) a very minor role for HS or SDN-1 in the orientation of the EMS spindle towards P_2 (supplementary material Fig. S6). An explanation for the differential requirement for HSPGs in EMS versus ABar is that in the case of EMS/P_2, the interacting cells are sisters and are in direct contact throughout their cell cycle. By contrast, reorientation of ABar towards its non-sister cell C requires formation of a new cell-cell contact, and therefore involves additional signal-concentrating or amplifying proteins such as SDN-1. The more elongated cell shape of EMS compared with ABar also suggests that EMS may be intrinsically

Development (2014) 141, 4354-4365 doi:10.1242/dev.113266

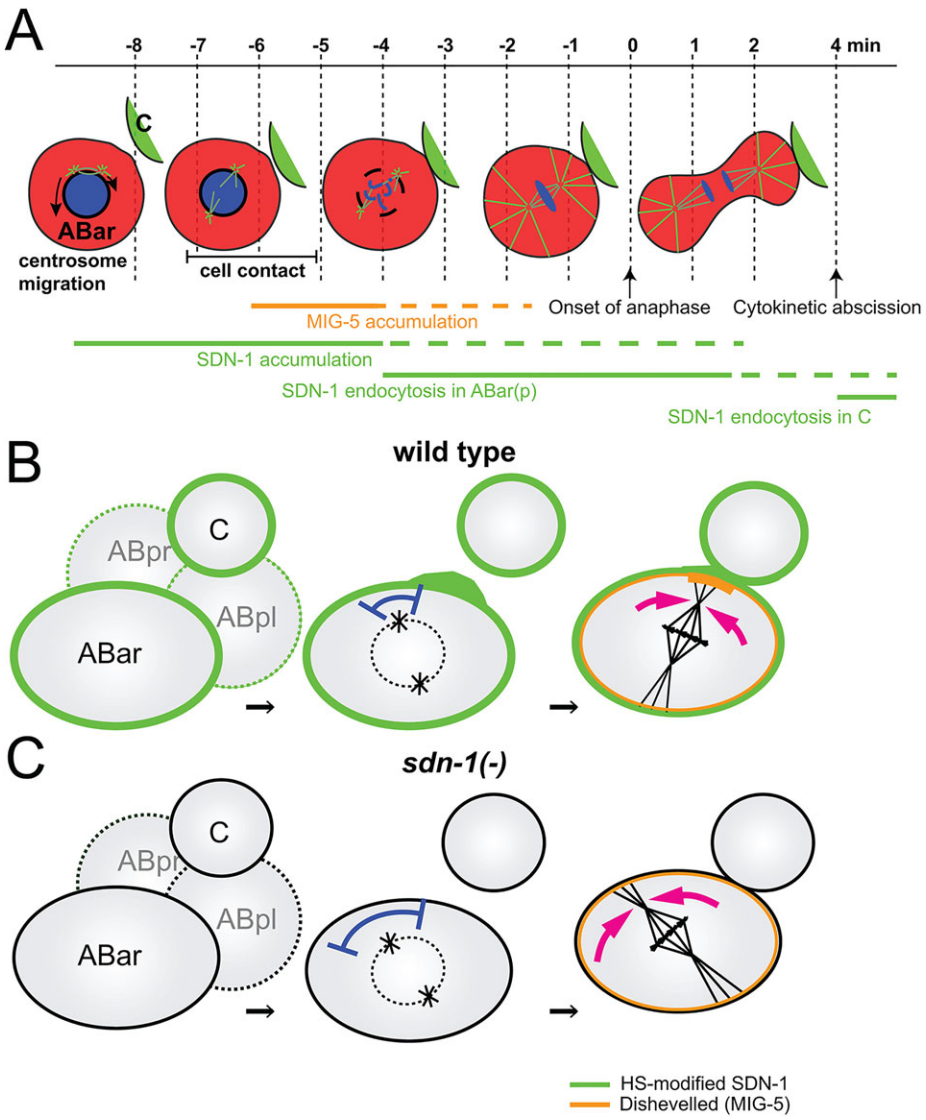

Fig. 8. Model for SDN-1 function in Wnt-dependent spindle orientation. (A) Timing of SDN-1 accumulation and endocytosis relative to ABar-C contact, MIG-5 accumulation and onset of anaphase. (B) In response to C-derived Wnt/MOM-2, SDN-1 (green) accumulates on the tip of ABar closest to C prior to cell-cell contact. The local accumulation of SDN-1 on the midbody remnant derived from ABp forms a Wnt 'signaling platform' that recruits downstream signaling molecules, such as Dsh/MIG-5, that then orient the ABar spindle towards the Wnt signaling platform. Alternatively, HS/SDN-1 may enhance availability of Wnt to facilitate signaling. (C) In the absence of SDN-1 the ABar spindle initially has a more variable orientation (blue bar), potentially reflecting a wider distribution of Wnt. In the absence of SDN-1, Wnt signaling platforms arise at ectopic locations and the ABar spindle orients toward these ectopically formed Wnt signaling platforms (magenta arrows), but Wnt signaling per se is not completely impaired in the absence of syndecan. We analyze the ABar spindle by tracking centrosomal asters (TBB-2::GFP) from –5.5 min, or analyze the ABar division angle, as defined by the orientation of daughter nuclei (HIS-72::GFP) 1 min after the onset of ABar anaphase.

more able to orient its spindle along its long axis (Hertwig's rule) even in the absence of positional cues (Goldstein, 1995).

Cytokinetic midbody remnants have been recently shown to contribute to orientation of mitotic spindles in the early embryo (Singh and Pohl, 2014). We found that total HS colocalized with midbody remnants on the ABar-C contact site. Some, but not all, midbody remnants contain total HS, suggesting that HSPGs may be selectively recruited into midbodies. Based on its location, the midbody remnant containing HS at the 8-cell stage seems to be that generated from the division of ABp. A previous study demonstrated that the midbody remnant from ABp is inherited by MS (Singh and Pohl, 2014), different from the dynamics of SDN-1. Possibly, SDN-1 is dissociated from the midbody remnant and is internalized into ABar or C during or after ABar mitosis.

An unexpected finding in this study is that SDN-1::GFP is apparently endocytosed into the signaling or receiving cells after spindle reorientation is complete. Endocytosis can either positively or negatively regulate Wnt signaling (Gagliardi et al., 2008). In *Xenopus*, syndecan 4 promotes Wnt/PCP signaling by inducing clathrin-mediated endocytosis of Rspo3, a positive Wnt modulator (Ohkawara et al., 2011). SDN-1 endocytosis in ABar might promote establishment or maintenance of the external cue for mitotic spindle orientation by recruiting the signaling complex to the acidic environment where the signal is activated (Niehrs and Boutros, 2010) or by sequestering unidentified negative regulators (Gagliardi et al., 2008). Alternatively, SDN-1 endocytosis by C may be involved in signal termination, as it was observed after ABar was in anaphase (Fig. 6C and supplementary material Fig. S5B). As SDN-1 is expressed at high levels in ABar and at lower levels in C, it is unclear whether the endocytosis of SDN-1 into C reflects endocytosis of SDN-1 on the C cell surface or bidirectional endocytosis of ABar-expressed SDN-1. In any case, the variable SDN-1 dynamics after accumulation may reflect a flexible or a context-sensitive signal modulation by SDN-1, which provides robustness in oriented cell division. Our experiments demonstrated the requirement of the SDN-1 cytoplasmic domain for regulation of ABar spindle orientation and SDN-1 internalization during mitosis. However, overexpression of SDN-1 lacking its cytoplasmic domain can rescue the ABar spindle orientation phenotype (supplementary material Fig. S5C,D). This suggests that the cytoplasmic domain modulates Wnt signaling rather than playing an essential role in signal transduction. Despite our findings that HS synthesis mutants display strong ABar spindle orientation defects, overexpression of a mutant form of SDN-1 predicted to lack GAG attachments was able to rescue *sdn-1* spindle orientation defects. This is reminiscent of previous findings where HSPG core proteins have been shown to

Development (2014) 141, 4354-4365 doi:10.1242/dev.113266

function independently of their HS side chains (Chanana et al., 2009; Kirkpatrick et al., 2006; Williams et al., 2010; Yan et al., 2009). However, we observed weak restoration of HS expression by overexpression of these SDN-1 mutants. There are several possible explanations for this unexpected result: SDN-1 itself might be modified at additional non-canonical sites; SDN-1 overexpression may induce the expression of other HSPG core-protein(s); or overexpression of an unmodifiable SDN-1 may result in inappropriate modification of other proteins not normally HS modified. The relationship of the GAG-dependent and core-protein functions of syndecans is complex (Eriksson and Spillmann, 2012) and an important avenue for future investigation.

Syndecans might be involved in mitotic spindle orientation in other situations when the signal is transiently transmitted from nascent cell contacts, e.g. in stem cell competition for niche occupancy (Johnston, 2009; Zhao and Xi, 2010). Syndecan 1 has been shown to promote proliferation of neural progenitor cells via canonical Wnt signaling (Wang et al., 2012). Because syndecans play major roles in wound healing and cancer progression (Alexander et al., 2000; Echtermeyer et al., 2001), such a context-specific mechanism may be involved in mitotic regulation of pathology in mammals, in addition to the well-established role of syndecans in cell migration.

MATERIALS AND METHODS

C. elegans strains

Strains used are summarized in supplementary material Table S1.

Plasmid construction and transgene generation

Plasmids were made by Gibson isothermal assembly (Gibson et al., 2009). To make the mutated nucleotides, site-directed mutagenesis was performed with Phusion polymerase (NEB). Mos-SCI was performed as described, using strains EG4322 and EG6699 (Frøkjaer-Jensen et al., 2008). Plasmids used are summarized in supplementary material Table S2.

Immunofluorescence

Embryos and gonads dissected from gravid adult worms were put on slides coated with poly-L-Lysine (Sigma-Aldrich), fixed in −20°C chilled methanol for 3 min, and treated with Heparin lyase II (Sigma-Aldrich) in buffer A [50 mM sodium acetate, 5 mM $CaCl_2$, 0.05% Tween-20 (pH 6.0)] for 2-3 h at 37°C, then blocked with TBS containing 0.2% Tween-20 and 5% BSA. After blocking, primary antibody was added and incubated overnight at 4°C. After washing twice with TBST, secondary antibody was added and incubated at room temperature (23-25°C) for 2 h. 3G10 antibody (US Biological) and anti-mouse IgG conjugated with Alexa 488 or 594 (Invitrogen) were used at 1:1000 dilution. 3D projections were made by Zen software (Zeiss) and images processed with Adobe Photoshop.

Measurement of total HS, SDN-1::GFP and MIG-5::GFP

For all fluorescence intensity measurement, we used maximum intensity projections of three *z*-slices. The first peak obtained by a line scan (perpendicular to the cell edge) was defined as a cell border and was used to select an ROI (3×3 pixels) on the cell border, then the mean intensity was acquired. To measure the intensity of SDN-1::GFP and MIG-5::GFP, fluorescence intensity ratios were calculated by dividing the mean intensity of GFP by that of PH::mCherry. Three-dimensional projections and measurements used ImageJ.

Confocal microscopy

Imaging was performed as previously reported (Giurumescu et al., 2012). Briefly, living embryos were observed on LSM510 or LSM710 confocal microscopes with 100× NA 1.46 oil immersion objectives. One to three embryos obtained from four or five gravid adults were imaged in each experiment. Each data set is derived from at least six experiments. Three-dimensional stacks were acquired every minute (for HIS-72::GFP) or every 30 s (other backgrounds). Thirty-five *z*-sections were collected at 0.85 µm intervals for HIS-72::GFP and TBB-2::GFP imaging. To avoid photobleaching and phototoxicity, only the dorsal one-third of the embryo (10 slices, 0.85 µm intervals for SDN-1::GFP and MIG-5::GFP) was scanned. Each embryo was imaged for ∼5-30 min, and we confirmed that this was not toxic to wild-type embryos. When calculating the ABxx division angle from HIS-72::GFP tracking, we compared cells 1 min after the chromosomes segregate, as this was the first time point when daughter nuclei positions are automatically determined by NucleiTracker4D.

RNAi

PCR was performed with primer containing T7 promoter sequence on the 5′ end using N2 (Bristol) total cDNA as a template. Primers used are listed below. Double stranded RNA (dsRNA) was synthesized using Megascript kit (Ambion), and then purified through a PCR Purification kit (QIAGEN). The purified dsRNA was injected at 1 mg/ml into young adult worms 22-28 h before analysis. Primers used for synthesis are summarized in supplementary material Table S3.

Data analysis

Semi-automated tracking of histone-labeled nuclei (transgene *zuIs178*) using NucleiTracker4D was performed as previously described (Giurumescu et al., 2012). We found that the NucleiTracker4D program could also track TBB-2::GFP-labeled centrosomal asters without further modifications. The angle between two vectors in 3D space is given by the inner product of two vectors:

$$\cos\ \theta = \frac{\vec{A}\cdot\vec{B}}{\|\vec{A}\|\|\vec{B}\|}.$$

After selecting four nuclei to generate two vectors, the formula is used to measure the angle between two selected vectors. The resulting angle θ ranges from 0 to 180°. We also want to measure the relative angle between the vector of two sister nuclei and the entire embryonic axis. The anterior-posterior axis (AP vector) was manually estimated from two projection images in *xy* plane and *xz* plane. The *x* and *y* points of the AP vector were decided by selecting two points in *xy* projection image. *z* points of the AP vector are decided by an identical method in an *xz* projection image. The angle between the AP vector and the vector of two sister nuclei is computed using the equation above.

To visualize the angles on a circular plot, the MATLAB toolbox CircStat (http://www.jstatsoft.org/v31/i10) is used. Codes are available upon request. As the range of angles used in this study was 0-180°, the angles were statistically treated as linear data. Statistical analysis used GraphPad Prism. We used the *F*-test for comparison of variance, Student's *t*-test and Fisher's exact test for comparison of two independent data sets. For multiple comparisons, we used one-way analysis of variance (ANOVA) followed by a Tukey or Dunnett post-hoc test for multiple comparison.

Acknowledgements

We thank all the members of the Jin and Chisholm laboratories for comments, advice and encouragement. We thank Jeffrey Esko, Yishi Jin and Hiroshi Nakato for comments, Kazuya Nomura for initial work on 3G10 immunostaining, Shaohe Wang for introducing us to Gibson cloning and plasmids, Claudiu Giurumescu for initial help with NucleiTracker4D, and the *Caenorhabditis* Genetics Center (CGC) for strains.

Competing interests

The authors declare no competing financial interests.

Author contributions

K.D. and A.D.C. designed the experiments, analyzed data and wrote the manuscript. K.D. performed the experiments. S.K. contributed analytical tools. A.D.C., S.M. and P.C.C. supervised the project.

Funding

The CGC is funded by the NIH Office of Research Infrastructure Programs [P40 OD010440]. K.D. was supported by a Japan Society for the Promotion of Science (JSPS) Post Doctoral Fellowship for Research Abroad. This work was supported by

a grant [R01 GM054657] from the National Institutes of Health to A.D.C. Deposited in PMC for release after 12 months.

Supplementary material

Supplementary material available online at
http://dev.biologists.org/lookup/suppl/doi:10.1242/dev.113266/-/DC1

References

Ai, X., Do, A.-T., Lozynska, O., Kusche-Gullberg, M., Lindahl, U. and Emerson, C. P., Jr (2003). QSulf1 remodels the 6-O sulfation states of cell surface heparan sulfate proteoglycans to promote Wnt signaling. *J. Cell Biol.* **162**, 341-351.

Alexander, C. M., Reichsman, F., Hinkes, M. T., Lincecum, J., Becker, K. A., Cumberledge, S. and Bernfield, M. (2000). Syndecan-1 is required for Wnt-1-induced mammary tumorigenesis in mice. *Nat. Genet.* **25**, 329-332.

Bishop, J. R., Schuksz, M. and Esko, J. D. (2007). Heparan sulphate proteoglycans fine-tune mammalian physiology. *Nature* **446**, 1030-1037.

Cabello, J., Neukomm, L. J., Günesdogan, U., Burkart, K., Charette, S. J., Lochnit, G., Hengartner, M. O. and Schnabel, R. (2010). The Wnt pathway controls cell death engulfment, spindle orientation, and migration through CED-10/Rac. *PLoS Biol.* **8**, e1000297.

Chanana, B., Steigemann, P., Jackle, H. and Vorbruggen, G. (2009). Reception of Slit requires only the chondroitin-sulphate-modified extracellular domain of Syndecan at the target cell surface. *Proc. Natl. Acad. Sci. USA* **106**, 11984-11988.

David, G., Bai, X. M., Van der Schueren, B., Cassiman, J. J. and Van den Berghe, H. (1992). Developmental changes in heparan sulfate expression: in situ detection with mAbs. *J. Cell Biol.* **119**, 961-975.

Echtermeyer, F., Streit, M., Wilcox-Adelman, S., Saoncella, S., Denhez, F., Detmar, M. and Goetinck, P. (2001). Delayed wound repair and impaired angiogenesis in mice lacking syndecan-4. *J. Clin. Invest.* **107**, R9-R14.

Eisenmann, D. M. (2005). Wnt signaling. In *Wormbook* (ed. The C. elegans Research Community) , http://www.wormbook.org.

Eriksson, A. S. and Spillmann, D. (2012). The mutual impact of syndecan-1 and its glycosaminoglycan chains–a multivariable puzzle. *J. Histochem. Cytochem.* **60**, 936-942.

Frøkjaer-Jensen, C., Davis, M. W., Hopkins, C. E., Newman, B. J., Thummel, J. M., Olesen, S.-P., Grunnet, M. and Jorgensen, E. M. (2008). Single-copy insertion of transgenes in *Caenorhabditis elegans*. *Nat. Genet.* **40**, 1375-1383.

Gagliardi, M., Piddini, E. and Vincent, J.-P. (2008). Endocytosis: a positive or a negative influence on Wnt signalling? *Traffic* **9**, 1-9.

Gibson, D. G., Young, L., Chuang, R.-Y., Venter, J. C., Hutchison, C. A., III and Smith, H. O. (2009). Enzymatic assembly of DNA molecules up to several hundred kilobases. *Nat. Methods* **6**, 343-345.

Gillies, T. E. and Cabernard, C. (2011). Cell division orientation in animals. *Curr. Biol.* **21**, R599-R609.

Giurumescu, C. A., Kang, S., Planchon, T. A., Betzig, E., Bloomekatz, J., Yelon, D., Cosman, P. and Chisholm, A. D. (2012). Quantitative semi-automated analysis of morphogenesis with single-cell resolution in complex embryos. *Development* **139**, 4271-4279.

Goldstein, B. (1995). Cell contacts orient some cell division axes in the *Caenorhabditis elegans* embryo. *J. Cell Biol.* **129**, 1071-1080.

Grana, T. M., Cox, E. A., Lynch, A. M. and Hardin, J. (2010). SAX-7/L1CAM and HMR-1/cadherin function redundantly in blastomere compaction and non-muscle myosin accumulation during *Caenorhabditis elegans* gastrulation. *Dev. Biol.* **344**, 731-744.

Habib, S. J., Chen, B.-C., Tsai, F.-C., Anastassiadis, K., Meyer, T., Betzig, E. and Nusse, R. (2013). A localized Wnt signal orients asymmetric stem cell division in vitro. *Science* **339**, 1445-1448.

Hardin, J. and King, R. S. (2008). The long and the short of Wnt signaling in *C*. elegans. *Curr. Opin. Genet. Dev.* **18**, 362-367.

Hudson, M. L., Kinnunen, T., Cinar, H. N. and Chisholm, A. D. (2006). *C*. elegans Kallmann syndrome protein KAL-1 interacts with syndecan and glypican to regulate neuronal cell migrations. *Dev. Biol.* **294**, 352-365.

Inaba, M. and Yamashita, Y. M. (2012). Asymmetric stem cell division: precision for robustness. *Cell Stem Cell* **11**, 461-469.

Johnston, L. A. (2009). Competitive interactions between cells: death, growth, and geography. *Science* **324**, 1679-1682.

Kachur, T. M., Audhya, A. and Pilgrim, D. B. (2008). UNC-45 is required for NMY-2 contractile function in early embryonic polarity establishment and germline cellularization in *C*. elegans. *Dev. Biol.* **314**, 287-299.

Kim, S., Ishidate, T., Sharma, R., Soto, M. C., Conte, D., Jr, Mello, C. C. and Shirayama, M. (2013). Wnt and CDK-1 regulate cortical release of WRM-1/beta-catenin to control cell division orientation in early *Caenorhabditis elegans* embryos. *Proc. Natl. Acad. Sci. USA* **110**, E918-E927.

Kirkpatrick, C. A., Knox, S. M., Staatz, W. D., Fox, B., Lercher, D. M. and Selleck, S. B. (2006). The function of a Drosophila glypican does not depend entirely on heparan sulfate modification. *Dev. Biol.* **300**, 570-582.

Kitagawa, H., Izumikawa, T., Mizuguchi, S., Dejima, K., Nomura, K. H., Egusa, N., Taniguchi, F., Tamura, J.-i., Gengyo-Ando, K., Mitani, S. et al. (2007). Expression of *rib-1*, a *Caenorhabditis elegans* homolog of the human tumor suppressor EXT genes, is indispensable for heparan sulfate synthesis and embryonic morphogenesis. *J. Biol. Chem.* **282**, 8533-8544.

Kleinschmit, A., Takemura, M., Dejima, K., Choi, P. Y. and Nakato, H. (2013). *Drosophila* heparan sulfate 6-O-endosulfatase Sulf1 facilitates wingless (Wg) protein degradation. *J. Biol. Chem.* **288**, 5081-5089.

Lancaster, M. A., Schroth, J. and Gleeson, J. G. (2011). Subcellular spatial regulation of canonical Wnt signalling at the primary cilium. *Nat. Cell Biol.* **13**, 700-707.

Lin, X. (2004). Functions of heparan sulfate proteoglycans in cell signaling during development. *Development* **131**, 6009-6021.

Lu, M. S. and Johnston, C. A. (2013). Molecular pathways regulating mitotic spindle orientation in animal cells. *Development* **140**, 1843-1856.

Merritt, C., Rasoloson, D., Ko, D. and Seydoux, G. (2008). 3′ UTRs are the primary regulators of gene expression in the *C*. elegans germline. *Curr. Biol.* **18**, 1476-1482.

Minniti, A. N., Labarca, M., Hurtado, C. and Brandan, E. (2004). *Caenorhabditis elegans* syndecan (SDN-1) is required for normal egg laying and associates with the nervous system and the vulva. *J. Cell Sci.* **117**, 5179-5190.

Mizumoto, K. and Sawa, H. (2007). Cortical beta-catenin and APC regulate asymmetric nuclear beta-catenin localization during asymmetric cell division in *C*. elegans. *Dev. Cell* **12**, 287-299.

Morgan, M. R., Hamidi, H., Bass, M. D., Warwood, S., Ballestrem, C. and Humphries, M. J. (2013). Syndecan-4 phosphorylation is a control point for integrin recycling. *Dev. Cell* **24**, 472-485.

Morin, X. and Bellaïche, Y. (2011). Mitotic spindle orientation in asymmetric and symmetric cell divisions during animal development. *Dev. Cell* **21**, 102-119.

Mullen, G. P., Rogalski, T. M., Bush, J. A., Gorji, P. R. and Moerman, D. G. (1999). Complex patterns of alternative splicing mediate the spatial and temporal distribution of perlecan/UNC-52 in *Caenorhabditis elegans*. *Mol. Biol. Cell* **10**, 3205-3221.

Muñoz, R., Moreno, M., Oliva, C., Orbenes, C. and Larraín, J. (2006). Syndecan-4 regulates non-canonical Wnt signalling and is essential for convergent and extension movements in *Xenopus* embryos. *Nat. Cell Biol.* **8**, 492-500.

Niehrs, C. and Boutros, M. (2010). Trafficking, acidification, and growth factor signaling. *Sci. Signal.* **3**, pe26.

Noatynska, A., Gotta, M. and Meraldi, P. (2012). Mitotic spindle (DIS)orientation and DISease: cause or consequence? *J. Cell Biol.* **199**, 1025-1035.

Ohkawara, B., Yamamoto, T. S., Tada, M. and Ueno, N. (2003). Role of glypican 4 in the regulation of convergent extension movements during gastrulation in *Xenopus laevis*. *Development* **130**, 2129-2138.

Ohkawara, B., Glinka, A. and Niehrs, C. (2011). Rspo3 binds syndecan 4 and induces Wnt/PCP signaling via clathrin-mediated endocytosis to promote morphogenesis. *Dev. Cell* **20**, 303-314.

Park, F. D. and Priess, J. R. (2003). Establishment of POP-1 asymmetry in early *C*. elegans embryos. *Development* **130**, 3547-3556.

Park, F. D., Tenlen, J. R. and Priess, J. R. (2004). *C. elegans* MOM-5/frizzled functions in MOM-2/Wnt-independent cell polarity and is localized asymmetrically prior to cell division. *Curr. Biol.* **14**, 2252-2258.

Pease, J. C. and Tirnauer, J. S. (2011). Mitotic spindle misorientation in cancer–out of alignment and into the fire. *J. Cell Sci.* **124**, 1007-1016.

Pohl, C. and Bao, Z. (2010). Chiral forces organize left-right patterning in *C. elegans* by uncoupling midline and anteroposterior axis. *Dev. Cell* **19**, 402-412.

Rhiner, C., Gysi, S., Fröhli, E., Hengartner, M. O. and Hajnal, A. (2005). Syndecan regulates cell migration and axon guidance in *C*. elegans. *Development* **132**, 4621-4633.

Sarrazin, S., Lamanna, W. C. and Esko, J. D. (2011). Heparan sulfate proteoglycans. *Cold. Spring Harb. Perspect. Biol.* **3**, a004952.

Sawa, H. and Korswagen, H. C. (2013). Wnt signaling in *C. elegans*. In *WormBook* (ed. The *C. elegans* Research Community), doi/10.1895/wormbook.1.7.2, http://www.wormbook.org.

Schwabiuk, M., Coudiere, L. and Merz, D. C. (2009). SDN-1/syndecan regulates growth factor signaling in distal tip cell migrations in *C. elegans*. *Dev. Biol.* **334**, 235-242.

Ségalen, M. and Bellaïche, Y. (2009). Cell division orientation and planar cell polarity pathways. *Semin. Cell Dev. Biol.* **20**, 972-977.

Siller, K. H. and Doe, C. Q. (2009). Spindle orientation during asymmetric cell division. *Nat. Cell Biol.* **11**, 365-374.

Singh, D. and Pohl, C. (2014). Coupling of rotational cortical flow, asymmetric midbody positioning, and spindle rotation mediates dorsoventral axis formation in *C*. elegans. *Dev. Cell* **28**, 253-267.

Strome, S., Powers, J., Dunn, M., Reese, K., Malone, C. J., White, J., Seydoux, G. and Saxton, W. (2001). Spindle dynamics and the role of gamma-tubulin in early *Caenorhabditis elegans* embryos. *Mol. Biol. Cell* **12**, 1751-1764.

Sumiyoshi, E., Takahashi, S., Obata, H., Sugimoto, A. and Kohara, Y. (2011). The β-catenin HMP-2 functions downstream of Src in parallel

with the Wnt pathway in early embryogenesis of C. elegans. *Dev. Biol.* **355**, 302-312.

Taelman, V. F., Dobrowolski, R., Plouhinec, J.-L., Fuentealba, L. C., Vorwald, P. P., Gumper, I., Sabatini, D. D. and De Robertis, E. M. (2010). Wnt signaling requires sequestration of glycogen synthase kinase 3 inside multivesicular endosomes. *Cell* **143**, 1136-1148.

Thorpe, C. J., Schlesinger, A., Carter, J. C. and Bowerman, B. (1997). Wnt signaling polarizes an early *C. elegans* blastomere to distinguish endoderm from mesoderm. *Cell* **90**, 695-705.

Tkachenko, E. and Simons, M. (2002). Clustering induces redistribution of syndecan-4 core protein into raft membrane domains. *J. Biol. Chem.* **277**, 19946-19951.

Walston, T., Tuskey, C., Edgar, L., Hawkins, N., Ellis, G., Bowerman, B., Wood, W. and Hardin, J. (2004). Multiple Wnt signaling pathways converge to orient the mitotic spindle in early *C.* elegans embryos. *Dev. Cell* **7**, 831-841.

Walston, T., Guo, C., Proenca, R., Wu, M., Herman, M., Hardin, J. and Hedgecock, E. (2006). *mig-5*/Dsh controls cell fate determination and cell migration in *C. elegans*. *Dev. Biol.* **298**, 485-497.

Wang, Q., Yang, L., Alexander, C. and Temple, S. (2012). The niche factor syndecan-1 regulates the maintenance and proliferation of neural progenitor cells during mammalian cortical development. *PLoS ONE* **7**, e42883.

Williams, E. H., Pappano, W. N., Saunders, A. M., Kim, M.-S., Leahy, D. J. and Beachy, P. A. (2010). Dally-like core protein and its mammalian homologues mediate stimulatory and inhibitory effects on Hedgehog signal response. *Proc. Natl. Acad. Sci. USA* **107**, 5869-5874.

Wu, M. and Herman, M. A. (2007). Asymmetric localizations of LIN-17/Fz and MIG-5/Dsh are involved in the asymmetric B cell division in *C.* elegans. *Dev. Biol.* **303**, 650-662.

Yan, D., Wu, Y., Feng, Y., Lin, S.-C. and Lin, X. (2009). The core protein of glypican Dally-like determines its biphasic activity in wingless morphogen signaling. *Dev. Cell* **17**, 470-481.

Zhao, R. and Xi, R. (2010). Stem cell competition for niche occupancy: emerging themes and mechanisms. *Stem Cell Rev.* **6**, 345-350.

Zhu, A. J. and Scott, M. P. (2004). Incredible journey: how do developmental signals travel through tissue? *Genes Dev.* **18**, 2985-2997.